THE JOURNAL OF PHYSICAL CHEMISTRY B

Article

pubs.acs.org/JPCB

The First Step of Amyloidogenic Aggregation

Fabio Castello,[†] Salvador Casares,[‡] Maria J. Ruedas-Rama,[†] and Angel Orte*[,†]

[†]Department of Physical Chemistry, Faculty of Pharmacy, University of Granada, Campus Cartuja, 18071 Granada, Spain

[‡]Department of Physical Chemistry, Faculty of Sciences, University of Granada, Campus Fuentenueva, 18071 Granada, Spain

Supporting Information

ABSTRACT: The structural and dynamic characterization of the on-pathway intermediates involved in the mechanism of amyloid fibril formation is one of the major remaining biomedical challenges of our time. In addition to mature fibrils, various oligomeric structures are implicated in both the rate-limiting step of the nucleation process and the neuronal toxicity of amyloid deposition. Single-molecule fluorescence spectroscopy (SMFS) is an excellent tool for extracting most of the relevant information on these molecular systems, especially advanced multiparameter approaches, such as pulsed interleaved excitation (PIE). In our investigations of an amyloidogenic SH3 domain of α-spectrin, we have found dynamic oligomerization, even prior to incubation. Our single-molecule PIE experiments revealed that these species are small, mostly dimeric, and exhibit a loose and dynamic molecular organization. Furthermore, these experiments have allowed us to obtain quantitative information regarding the oligomer stability. These pre-amyloidogenic oligomers may potentially serve as the first target for fibrillization-prevention strategies.

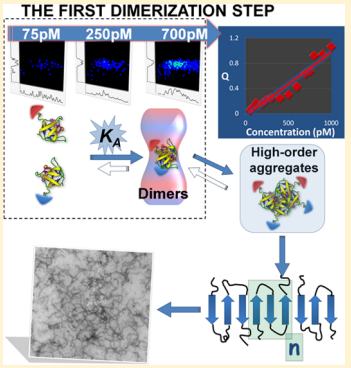

INTRODUCTION

The high impact of neurodegenerative diseases, including Alzheimer's, Parkinson's, and many others,[1,2] on both the quality of life of those affected and the world economy is currently one of the major issues in the field of biomedicine. The common hallmark of these diseases is the deposition of fibrillar proteinaceous plaques called amyloid fibrils. The structural and dynamic characterization of the on-pathway intermediates involved in the mechanism of amyloid fibril formation remains to be determined. These early oligomeric structures represent one of the most interesting therapeutic targets because they play a central role in the neuronal toxicity of amyloid plaques.[3] Understanding the nature and formation mechanism of these aggregates is therefore crucial for the development of chemical or biological treatments that successfully reduce the strong impact of amyloid diseases.

One of the major difficulties hindering the study of the mechanism of amyloid fibril formation via conventional techniques is the transient nature of the heterogeneous population of the various formed species.[4−6] Conventional biophysical tools for the study of amyloid fibril formation provide bulk information on the ensemble of the population, which is typically sufficient to assess the overall aggregation kinetics and evaluate hypotheses for broad mechanisms of aggregation. This family of techniques typically comprises thioflavin T fluorescence emission and turbidimetry, among others. Nevertheless, these techniques are not sufficient to unravel the intrinsic heterogeneity of preamyloid aggregates. Additional knowledge on the population of these aggregates has been acquired using alternative approaches, which allow for a more complete characterization than classical techniques. For example, dynamic light scattering (DLS)[7] and fluorescence correlation spectroscopy[8] provide insights into the distributions of species based on the diffusional properties. Imaging techniques, such as atomic force microscopy,[9] total internal reflection fluorescence microscopy,[10] and superresolution fluorescence microscopy,[11] have been recently employed to directly probe the shape of aggregates, monitor fibril growth, and directly visualize the localization of aggregates within live cells.

Among novel biophysical techniques, single-molecule fluorescence spectroscopy (SMFS) allows for the investigation of biomolecular interactions at the molecular level. The ability to individually probe molecules within a large population provides the direct and exciting advantage of immediately revealing the heterogeneity of the population.[12,13] These advantages offer new possibilities to elucidate the mechanism for the amyloid fibril formation process. Direct detection of aggregated species has been achieved utilizing dual-color excitation SMFS schemes[14] and multiparametric single-molecule spectroscopy.[15] Burstwise analysis of coincident single-molecule fluorescence events upon dual-color excitation[14] has provided in-depth information on the size distributions and kinetics of aggregation.[16] This approach has been successfully applied to studies on disease-related proteins. The aggregate populations, thermodynamic properties, and the effect of aggregation-inhibiting chaperonins have been studied for amyloid-β peptides,[17] which represent the primary component of amyloid plaques in Alzheimer's disease. Similarly, monitoring the kinetics of neuroserpin polymerization at the single-molecule level has provided insights into the underlying aggregation

Received: February 27, 2015
Revised: June 1, 2015

ACS Publications © XXXX American Chemical Society

DOI: 10.1021/acs.jpcb.5b01957
J. Phys. Chem. B XXXX, XXX, XXX−XXX

mechanism in familial encephalopathy with neuroserpin inclusion bodies.[18]

The picture of amyloid aggregation is even more complex. The complete energy landscape of protein aggregation may include several types of protein−protein interactions, which may or may not give rise to amyloidogenic aggregation and toxicity.[3,6,19] Various types of oligomers can precede amyloid fibril growth, although fibril growth only occurs after a two-step nucleation process at physiological concentrations.[20] Importantly, recent studies have identified differential cytotoxicity caused by different types of oligomers.[21,22] SMFS studies have provided additional information on the structural arrangement of the aggregates by monitoring the efficiency of the fluorescence resonance energy transfer (FRET) between a donor dye and an acceptor fluorophore within the same[23,24] or separate α-synuclein monomers, which are the major components of Lewy bodies in Parkinson's disease.

Herein, we go a step beyond previous studies by investigating the oligomeric species implicated in amyloid fibril formation at the single-molecule level using an advanced multiparameter SMFS technique that employs a dual-color pulsed interleaved excitation (PIE) scheme.[25,26] The SMFS-PIE technique provides the best results for the determination of the FRET efficiency because it sums orthogonal dimensions of information about single-molecule events, thus providing more accurate information on the oligomers. In this study, we focus on the SH3 domain of α-spectrin, which is a model protein domain that forms amyloid fibrils at low pH and in the presence of salt.[27] Specifically, we investigate the effect of an amyloidogenic-prone mutation, N47A, which exhibits enhanced aggregation.[28]

EXPERIMENTAL METHODS

Protein Preparation and Labeling. A modified mutant of the N47A variant of the α-spectrin SH3 domain was designed by introducing a six-residue tag (Gly-Ser-Gly-Ser-Gly-Cys) with the Cys residue at the C-terminus of the domain. We used the pBAT4:N47A-SH3 plasmid containing the modified domain. The protein was overexpressed using this plasmid in *Escherichia coli* BL21(DE3) cells. The cells were lysed, and the protein was recovered by ammonium sulfate precipitation at 75% saturation. The protein was solubilized, purified using size exclusion chromatography, dialyzed extensively, and lyophilized for storage until analysis (see the Supporting Information for additional experimental details). The protein purity was confirmed by SDS-PAGE and HRMS Q-TOF analyses. The addition of the six-residue tag at the C-terminus does not appreciably alter the ability of the construct to form amyloid fibrils (Figure S1 in Supporting Information).[8]

Labeling of the protein at the terminal Cys residue with maleimide-reactive forms of ATTO dyes was performed according to the manufacturer's instructions (see Supporting Information). The N47A-SH3-A488 (labeled with ATTO 488, ATTO-TEC GmbH, Germany) and N47A-SH3-A647N (labeled with ATTO 647N, ATTO-TEC GmbH) samples were purified and lyophilized for storage. Prior to analysis, the samples were diluted in 100 mM Gly buffer and stored in the dark at 4 °C.

For the aggregation experiments, the lyophilized N47A-SH3 samples were dissolved in an aggregation buffer containing 0.1 M glycine and 0.1 M NaCl at pH 3.2 and centrifuged for 2 min at 14 000 rpm in a microcentrifuge to remove preexisting fibrillar species. The aggregation buffer was filtered through 0.02 μm filters (Whatman) prior to use. The protein concentration was determined using UV−vis spectroscopy as described in the Supporting Information. For amyloid aggregation, the two labeled proteins were mixed at a 1:1 ratio to a total protein concentration of 32 μM in the aggregation buffer at 37 °C.[7,27]

SMFS-PIE Technique. The SMFS-PIE instrument is based on a MicroTime 200 apparatus (PicoQuant GmbH, Germany) and has been previously described.[8] Briefly, the excitation sources were two spatially overlapped pulsed lasers (<100 ps, fwhm) at 470 and 635 nm, with the latter temporally delayed by 24 ns to achieve PIE. The overall excitation pulse frequency was 20 MHz. The excitation lasers were focused into 60 μL of sample solution deposited on a microscope cover glass through a high numerical aperture oil-immersion objective (Plan Achromat 100×/1.40, Olympus). The fluorescence photons were collected, imaged onto a 75 μm pinhole, filtered, and separated into two detection channels—one for A488 (donor) fluorescence and one for A647N (FRET and directly excited acceptor) fluorescence—after which they were directed into two single-photon avalanche diodes. The photon detection events were temporally tagged (time-tagged time-resolved, TTTR)[29] to facilitate the reconstruction of the fluorescence decay traces and establish the temporal time gates for filtering the burst traces (Figure 1).[25,26] Additional instrumental details are described in the Supporting Information.

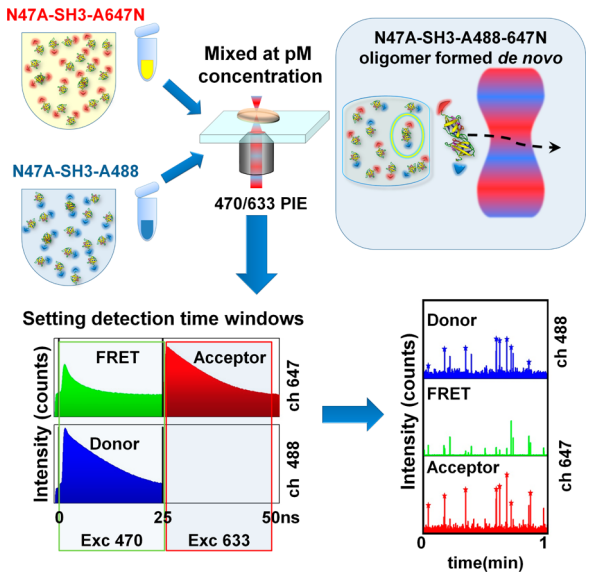

Figure 1. Schematic of the SMFS-PIE experiments. Dual-color PIE allows for the setting of time gates on the nanosecond time scale to filter the fluorescence signal into three traces: F_{A488} (donor), F_{FRET}, and F_{A647N} (directly excited acceptor).

The time filtering allows for the definition of three fluorescence traces: donor (F_{A488}), FRET (F_{FRET}), and directly excited A647N (F_{A647N}). Here, F_X denotes the fluorescence signals corrected for the background, direct excitation of the acceptor by the donor laser, and crosstalk. The selection and counting of single-molecule bursts were performed by setting a threshold value of 15 kHz for F_{A488} and F_{A647N}. Coincident and FRET events are determined when a burst is detected simultaneously in F_{A488} and F_{A647N}. Using the time gating and the PIE scheme removes the influence of the ubiquitous "zero peak" in FRET histograms.[25,26] We employed a validated

DOI: 10.1021/acs.jpcb.5b01957
J. Phys. Chem. B XXXX, XXX, XXX−XXX

probabilistic method to remove the contribution from coincident events caused by the pure chance encounter of two nonassociated molecules simultaneously in the probe volume.[14] The parameters of interest were the association quotient, Q, defined as the fraction of coincident events;[14] the FRET efficiency, E, and the ratio F_{A488}/F_{A647N} of the coincident events; and the donor lifetime, τ_{A488}, obtained burstwise by fitting the fluorescence decay to a single-exponential decay function using the maximum likelihood estimator to ensure accurate fitting with a low number of photons.[30] The analyses of the single-molecule traces (see Supporting Information for additional details) were performed using in-house-coded scripts within the SymPhoTime software (PicoQuant).

To study the formation of protein dimers at the single-molecule level, the N47A-SH3-A488 and N47A-SH3-A647N samples were individually stored in the dark (at a concentration between 20 and 40 μM) at 4 °C. Several dilution steps were performed on the aggregation buffer (0.1 M glycine, 0.1 M NaCl, pH 3.2). The two constructs were mixed (1:1 ratio) only during the last of these steps immediately prior to performing the SMFS-PIE measurement. This process ensures that any aggregate (containing both fluorescent tags) detected in the SMFS-PIE experiments has been readily formed *de novo*. The total protein concentration in the different measurements ranged from 50 to 1000 pM. The microscope cover glasses were washed three times with 95% ethanol, air-dried, and then pretreated with a 15 μM solution of bovine serum albumin (BSA) for 20 min. The unbound BSA was removed by aspiration and discarded. Fluorescence traces of each sample were collected for a total measurement time of 120 min.

Fluorescence Lifetime Imaging Microscopy. Fluorescence lifetime imaging microscopy (FLIM) images were recorded using an identical setup as described for the SMFS-PIE experiments but with laser focusing just above the glass surface to image the deposited molecules on the slide. The PIE scheme in FLIM permits the acquisition of three simultaneous images from a single scan using the aforementioned time gates for the definitions of F_{A488}, F_{FRET}, and F_{A647N}. Samples of N47A-SH3-A488 and N47A-SH3−647N (1:1 ratio) at a total concentration of 32 μM in the aggregation buffer at 20 °C were mixed and diluted 10 000-fold immediately prior to direct deposition onto the pretreated slide for FLIM image acquisition. The microscope cover glasses (Thermo Fisher Scientific, MENZEL-GLÄSER, Brawnschweig, Germany) were thoroughly cleaned using a previously described procedure[31] and stored in distilled water. Immediately prior to use, the slides were washed with ethanol and briefly air-dried.

A wide area (between 10 and 15 μm^2) was raster scanned with an $x-y$ piezo-driven device to set the region of interest (ROI). The images were obtained with a spatial resolution of 512 × 512 pixels using a collection time of 0.60 ms/pixel and a time resolution of 116 ps per channel in the single-photon timing scale (microtime). At least 20 images were collected from various areas for each sample.

The analysis of the FLIM images was identical to that used in the single-molecule fluorescence traces but in a pixel-by-pixel fashion.

RESULTS AND DISCUSSION

Various Types of N47A-SH3 Oligomers. To study the protein aggregation at the single-molecule level, stoichiometric amounts of the labeled constructs (50% of N47A-SH3-A488 and 50% of N47A-SH3-A647N labeled proteins) were incubated to form amyloid fibrils. The aggregate-forming interaction between monomers including the donor (ATTO 488) and the acceptor fluorophore (ATTO 647N) can be detected at the single-molecule level using PIE and FRET (Figure 1). The presence of the fluorophores did not appreciably hinder the capacity of the proteins to form mature amyloid fibrils, which are clearly visible in electron micrographs after 3 days of incubation at a total concentration of 32 μM (Figure S1). Both labeled and unlabeled N47A-SH3 fibrils exhibited a curly shape, which is a typical feature of fibril growth controlled by heterogeneous nucleation,[32] Similarly, the fluorophores did not vary the structural integrity of the N47A-SH3 construct, as demonstrated by circular dichroism (CD) analysis (Figure S2 and Table S1).

Several aliquots of these incubated samples were taken at different incubation times and analyzed at the single-molecule level using SMFS-PIE. The single-molecule correlograms revealed the presence of at least two different populations of oligomeric species based on the intraoligomer FRET efficiency (Figure 2): a low-FRET population that does not exhibit a

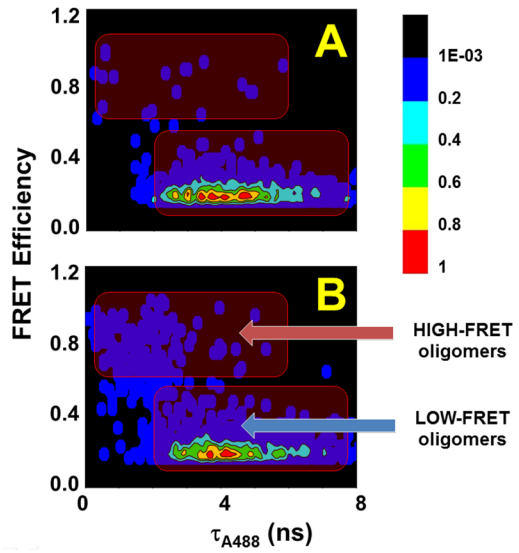

Figure 2. Single-molecule correlogram of the FRET efficiency versus the donor fluorescence lifetime. (A) N47A-SH3-A488 and N47A-SH3-647N protein samples mixed at a 1:1 ratio at a total concentration of 800 pM and measured without incubation. (B) N47A-SH3-A488 and N47-SH3-A647N samples mixed at a 1:1 ratio and incubated at 32 μM for 8 h.

significant change in the donor lifetime and a high-FRET population characterized by a reduction in τ_{A488}. Interestingly, the most striking feature of these results is that the oligomers exhibiting a low FRET efficiency were detected at the initial stage of the oligomerization reaction, even in the absence of incubation and when the samples were mixed at low concentrations (Figure 2A). This result is surprising and important because these very rapidly formed oligomers may constitute the first step of amyloidogenic nucleation, and hence, they may be a potential target in the first line of therapy against amyloidogenic nucleation. Therefore, we fully characterized these early aggregates at the molecular level.

Characterization of Early Oligomers. We hypothesize that the oligomers in this early population are both dynamic and labile in nature because they are ubiquitous, even in the absence of incubation. To investigate their stability, we

DOI: 10.1021/acs.jpcb.5b01957
J. Phys. Chem. B XXXX, XXX, XXX−XXX

performed a series of SMFS-PIE experiments in which the labeled constructs, N47A-SH3-A488 and N47A-SH3-A647N, were kept separated at low concentrations and mixed in aggregation buffer (0.1 M glycine, 0.1 M NaCl, pH 3.2) immediately prior to the measurement triggers. These experimental conditions ensured that all of the oligomers that include both N47A-SH3-A488 and N47A-SH3-A647N are readily formed *de novo* within the time frame of the SMFS-PIE measurement and confirm the dynamic nature of these oligomers. This dynamic population of aggregates allows for the oligomer formation equilibrium to be studied by modifying the protein concentration as the critical parameter in the association equilibrium of the oligomers. Therefore, we studied the interaction between N47A-SH3-A488 and N47A-SH3-A647N at different concentrations at the single-molecule level, specifically, between 50 and 1000 pM. Moreover, the low protein concentration used during the measurements prevents any further amyloidogenic aggregation. The detection of the formation of aggregates was confirmed using the coincidence criterion, i.e., simultaneous single-molecule fluorescent bursts detected in the A488 channel and in the A647N channel.[14] The SMFS-PIE technique also provides the fluorescence lifetime of the fluorophore for each individual burst,[25,26] which is particularly important for the recovery of accurate FRET efficiency values from the decrease in the lifetime of the donor (τ_{A488}).[33] Three key pieces of information are obtained from the coincident events in these experiments: the A488 fluorescence lifetime distribution; the distribution of the A488 and A647N intensity ratio, F_{A488}/F_{A647N}; and the fraction of coincident events, i.e., the association quotient, Q (see Experimental Methods and Supporting Information for details). The correlograms of F_{A488}/F_{A647N} vs τ_{A488} (Figure 3A) visualize the amount of oligomers formed at each concentration, the distribution of the stoichiometries, and the intraoligomer FRET efficiency. These correlograms revealed a population of oligomers without a significant change in the donor fluorescence lifetime, which was approximately 4 ns. This low FRET efficiency suggests a loose, broad structural arrangement involving the protein-retaining residual structure at the working pH (as confirmed by CD analysis, Figure S2). Indeed, the N47A-SH3 domain can be considered as a barrel-shaped domain of 25 Å in both axes (PDB entry 1QKX; see Figure S3).[34] The unstructured, flexible tail at the C-terminus and the dye linker add 25.6 Å. Using such a model to construct a model dimer that includes A488 and A647N and assuming equally probable but random orientations of the two monomers yields an average interfluorophore distance of 72.4 ± 18.9 Å (see Supporting Information and Figure S4 for details). This distance corresponds to an average FRET efficiency of 0.11 ± 0.15 (with R_0 = 51 Å).[35] Therefore, this model is in agreement with our observations. Similarly, the single-molecule correlograms (Figure 3A) reveal that the $\log(F_{A488}/F_{A647N})$ distribution was centered at zero, which indicates a 1:1 stoichiometry of the A488- and A647N-labeled proteins;[14] thus, the majority of the detected oligomeric species are dimers. Finally, Q is proportional to the amount of oligomers found in solution.[14] The relationship between Q and the total protein concentration (Figure 3B) yields quantitative information on the oligomerization equilibrium and serves as a tool to quantify the equilibrium constant (see below).

The detection of these oligomers was striking, particularly at the low concentrations employed. Therefore, we performed a series of complementary experiments to confirm the presence

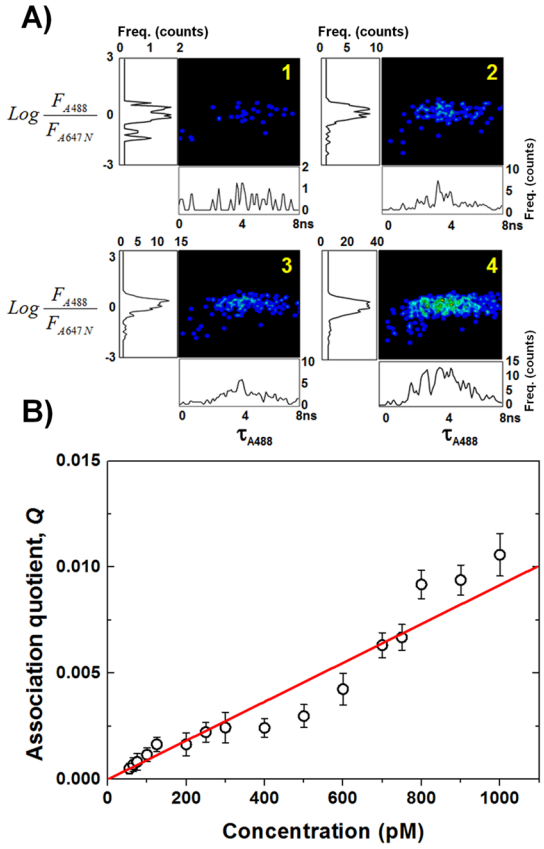

Figure 3. (A) Correlograms of the F_{A488}/F_{A647N} ratio (logarithmic scale) versus the donor fluorescence lifetime (τ_{A488}) of the single-molecule coincident events from mixtures of N47A-SH3-A488 and N47A-SH3-A647N (1:1 ratio) at total protein concentrations of (1) 75, (2) 250, (3) 400, and (4) 700 pM. (B) Association quotient, Q, versus the total labeled protein concentration. The error bars correspond to the propagation of the uncertainties in the parameters involved in the estimation of Q, and the experimental data were fitted to a straight line.

of oligomers prior to incubation. We employed a cross-linking agent (glutaraldehyde 25% (w/v) for 3 min) to detect labile oligomeric species present at a protein concentration of 60 μM in the aggregation buffer and a temperature of 20 °C. We performed these experiments with the unlabeled construct (with the addition of a reducing agent, 5 mM DTT, to avoid undesired disulfide bonds), the N47A-SH3-A488, and the N47A-SH3-A647N. SDS-PAGE was used to analyze the species present (see Supporting Information and Figure S5). These experiments revealed a ladder of species in which the main band corresponded to the monomeric form, with higher-order species also detected. These oligomers were detected in all of the samples tested, with or without a fluorescent probe attached, indicating a genuine oligomerization process carried out by the protein. Interestingly, the presence of SDS resulted in the disaggregation of the oligomers when the cross-linking agent was not used. This result supports the theory that these associations are relatively weak and noncovalent in nature. We also performed DLS measurements (see Supporting Information and Figure S6), which indicated the formation of oligomers of either labeled construct at 20 °C in the absence of prior incubation at protein concentrations of 60 and 120 μM in the aggregation buffer. The unlabeled N47A-SH3 domain containing the GSGSGC tag exhibited two major components

DOI: 10.1021/acs.jpcb.5b01957
J. Phys. Chem. B XXXX, XXX, XXX−XXX

with apparent average hydrodynamic radii (R_h) of 1.8 and 2.3 nm (Figure S6). According to Wilkins et al.,[36] the value of 1.8 nm could be assigned to an expanded monomeric form, which may be a necessary step prior oligomerization. This value is in contrast with the size of a compact monomer, R_h = 1.6 nm, previously reported for the same N47A-SH3 domain.[28] Following the same rationale, the value of 2.3 nm cannot be assigned to either an unfolded monomer ($R_h \approx 2.45$ nm) or compact dimer ($R_h \approx 1.97$ nm); instead, this R_h value would be more consistent with an expanded dimeric species, as previously stated by Morel et al.[28] These results appear to be independent of the protein concentration. However, the presence of the labeling dye does not appear to alter the ability of the protein to oligomerize, but it does make the process faster, as inferred because the 1.8 nm species is only present in N47A-SH3-A647N samples at low concentrations (60 μM) but is not present in the N47A-SH3-A488 variant or the two variants mix at both concentrations tested (Figure S6).

The results obtained with these ensemble techniques (SDS-PAGE and DLS) were fully consistent with those obtained at the single-molecule level, despite the difference in the concentration ranges tested. Importantly, whereas dimeric aggregates were primarily observed in the single-molecule experiments, larger aggregates are also observed when using macroscopic methods, i.e., at higher concentrations. This is consistent with the concentration dependence of the aggregation mechanism, as expected for any amyloidogenic process.

To visually inspect the formation of the preincubated oligomers, we performed fluorescence lifetime imaging microscopy (FLIM) with a dual-color PIE scheme (PIE-FLIM). This technique has the advantage of allowing the application of time-gate filters (Figure 1) to reconstruct three simultaneous FLIM images: donor, FRET, and directly excited acceptor images. We mixed N47A-SH3-A488 and N47A-SH3-A647N (ratio 1:1) at a total protein concentration of 32 μM into the aggregation buffer. After dilution to a final protein concentration of 280 pM (single-molecule level) and deposition onto a microscope glass slide, the single proteins were imaged. The analysis of the images (see Figure 4A for a representative image) revealed several events due to donor-only and acceptor-only proteins. The presence of aggregates was confirmed by the simultaneous colocalization of single molecules in the donor, the acceptor, and the FRET image (circled molecules in Figure 4A). Significantly, the fluorescence lifetime distributions of the donor within the aggregates (Figure 4C) did not appreciably differ from the donor-only monomers (Figure 4B), supporting the notion of a low FRET efficiency and therefore a loose structural arrangement. To quantify the FRET efficiency of such oligomers, we collected images of A488-labeled N47A-SH3 to obtain the lifetime distribution of the donor dye in the absence of an acceptor (Figure S7). The average lifetime of N47A-SH3-A488 on glass slides in the absence of an acceptor was 3.40 ± 0.10 ns. The Gaussian fit of the oligomer population in Figure 4C is centered at 2.45 ns, thus representing an average FRET value of 0.28 (= 1 − 2.45/3.40), confirming the low-FRET nature of these oligomers. The lifetime histogram in Figure 4C exhibits an additional peak centered at 2.1 ns from oligomers undergoing a slightly higher FRET than the remaining aggregates. Such a population is still in the low-FRET regimen, with E = 0.38. Larger FRET efficiency values of approximately 0.7 would exhibit a donor lifetime of approximately 1.0 ns. Therefore, this peak in the

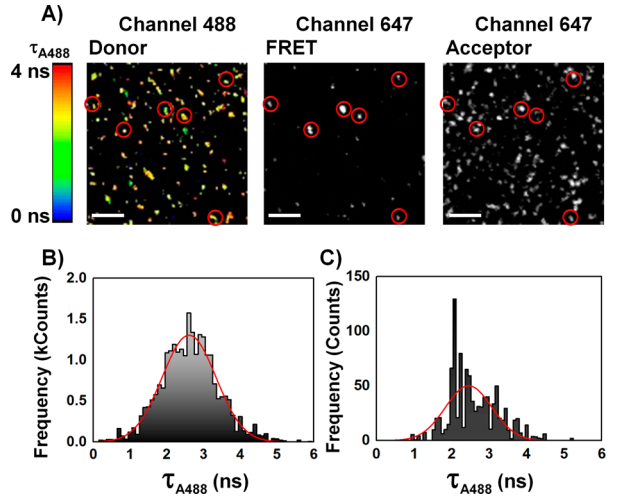

Figure 4. PIE-FLIM experiments. (A) Donor (F_{A488}), FRET (F_{FRET}), and directly excited A647N (F_{A647}) images of a mixture of N47A-SH3-A488 and N47A-SH3-A647N (ratio 1:1) in the aggregation buffer at a total protein concentration of 32 μM and diluted down to 280 pM for imaging. The circles indicate colocalized spots that contain all three events: A488, FRET, and directly excited A647N. The donor FLIM image is colored using a pseudocolor scale ranging from 0 to 4 ns. The scale bars represent 2.4 μm. (B) A488 fluorescence lifetime distribution among non-colocalized molecules (donor-only), corresponding mainly to N47A-SH3-A488 monomers. (C) A488 fluorescence lifetime distribution among protein aggregates (circled regions) collected over 10 images.

lifetime distribution is only caused by random donor−acceptor distances in low-FRET, loosely structured oligomers. All these results were in good agreement with those of the single-molecule experiments.

An important aspect to consider regarding these oligomers is their actual role on the mechanism of amyloid fibril formation, i.e., whether they are on- or off-pathway aggregates. Unlike other amyloidogenic proteins such as transthyretin that form oligomers in the native state and whose oligomers must be broken apart before amyloid aggregation, N47A-SH3 is a monomer in the native state.[37] We detected the formation of these rapidly forming aggregates when the protein is solved at low-pH and high-salt conditions. Previous aggregation studies on the N47A-SH3 mutant, although performed at higher protein concentrations than considered here, suggested that the bulk aggregation kinetics can be explained through a rate-limiting step involving a rapid pre-equilibration of the conformational opening of the monomer and subsequent oligomerization.[32] Our work sheds light on this mechanism because our results illustrate this suggested mechanism at the molecular level. Moreover, a recent computational study by Knowles, Frenkel, and colleagues[20] highlighted the necessary two-step nucleation mechanism for amyloid fibril formation in the physiological concentration regimen such as the micromolar concentrations employed herein. This protein concentration range is considerably lower than traditional studies on amyloid fibril formation. According to these authors, at low peptide concentrations, nucleation can only be achieved through nonspecific attractions between soluble monomers in a two-step nucleation process. Our results provide experimental support for this model through the use of a highly sensitive SMFS technique to overcome the challenge of the low concentrations of the formed oligomers. Our technique

DOI: 10.1021/acs.jpcb.5b01957
J. Phys. Chem. B XXXX, XXX, XXX−XXX

provides direct detection of the oligomers and is able to obtain quantitative thermodynamic information on these oligomers, as detailed in the next section.

Determination of the Equilibrium Constant for Dimer Formation. After the presence of genuine oligomers prior to efficient amyloidogenic incubation was validated, more detailed and quantitative information was obtained from the SMFS-PIE experiments. The association quotient, Q, exhibited a concentration dependence (Figure 3B), which clearly indicates the establishment of a dynamic equilibrium between the monomers and aggregates. This equilibrium is extremely important for the amyloid fibril formation process because it represents the first step of amyloidogenic aggregation. Notably, the two labeled proteins had been mixed at very low concentrations; therefore, any aggregate formed that includes both fluorescent tags was produced during the time course of the measurement. Intuitively, and based on the encounter probability, most of the dual-labeled aggregates must be dimers because the probability of forming higher-order species is very low. Therefore, using the Q values, we can estimate the value of the association equilibrium constant, K_A, for the formation of the dimers, i.e., the first step of amyloidogenic aggregation. K_A can be defined as follows:

$$K_A = \frac{[D]}{[M]^2} \tag{1}$$

where $[D]$ and $[M]$ represent the concentrations of dimers and monomers, respectively.

As previously described,[14,16] the association quotient, Q, is proportional to the fraction of molecules containing the two fluorescent tags. In this case, as the number of aggregates is low

$$Q \propto \frac{[D]}{[M]} \tag{2}$$

The proportionality factor is determined by the efficiency of the instrumental detection of coincident fluorescence bursts. We determined this detection efficiency using 100% dual-labeled 45-base-pair dsDNA, which yielded a detection efficiency of 18.6 ± 0.7%. Therefore, the conversion factor to obtain the fraction of dual-labeled molecules from Q is 5.4 ± 0.2. Furthermore, another important correction must be accounted for only dimers containing both A488 and A647N can be detected by our method. The probabilistic binomial coefficients indicate that these dimers are only 50% of the total dimers, as there is a 25% probability of finding a dimer with two A488-labeled monomers and a 25% probability of finding a dimer with two A647N-labeled monomers. Therefore, we must also consider the fraction of dimers that cannot be detected by adding a factor of 2. Considering both of these corrections, the proportionality factor can be inserted into eq 2, as follows:

$$\frac{[D]}{[M]} = 2 \cdot 5.4 \cdot Q \tag{3}$$

Using eqs 1 and 3, we can then establish the following relationship between Q and K_A:

$$Q = \frac{K_A \cdot [M]}{2 \cdot 5.4} \tag{4}$$

Equation 4 suggests that the plot of Q versus the total monomer concentration should follow a straight line. Because our experimental results fit this model very well (Figure 3B), the apparent association equilibrium constant K_A can be recovered from the slope of the linear fit. The slope of the plot in Figure 3B is $(9.2 \pm 0.7) \times 10^{-6}$ pM^{-1}, which provides a value for K_A of $(9.9 \pm 0.8) \times 10^7$ M^{-1} (the associated error was obtained from the error propagation of the uncertainties in the slope and the detection efficiency factor). It is sometimes more intuitive to consider the dissociation equilibrium (the inverse reaction), which has a corresponding equilibrium constant, K_D, defined as $1/K_A$. The K_D value obtained was 10.1 ± 0.9 nM, which clearly indicates that the protein tends to aggregate at concentrations above 10 nM. This result accounts for the formation of larger oligomer aggregates observed using macroscopic techniques and reveals that the aggregates formed in the first step of amyloid aggregation are highly stable.

The value for K_A obtained here was considerably larger (2 orders of magnitude) than that reported by Ruzafa et al.[32] for the N47A-SH3 domain. These authors analyzed aggregation kinetics from classic bulk experiments (e.g., ThT and ANS fluorescence, CD, DLS) through a simple mechanistic model involving equilibrium between the native and unfolded monomers and a partially folded intermediate monomer, along with an aggregation/elongation step that was governed by the equilibrium constant K_A. Although fitting of the experimental data to this model was occasionally over-parametrized and could not converge without fixing some of the equilibrium constants involved, a K_A value of $(2.5 \pm 0.5) \times 10^5$ was obtained. The reasons behind this apparent disagreement between parameters that should be comparable may lie on the differences in the concentration regimens employed in either one of the studies. At the high protein concentrations used by Ruzafa et al. (approximately 1 mM), the association events may be dominated by amyloid nucleation via a one-step nucleation mechanism. In fact, Ruzafa and colleagues proposed a one-step nucleation kinetic model to fit the experimental data. Therefore, the value for K_A estimated by these authors may represent the association equilibrium when aggregation is governed by one-step nucleation. This study focuses on individual association events that occur at sub-nanomolar concentrations, detected at the molecular level. We cannot rule out the possibility that the presence of the dyes contributes to enhancing the value of K_A, as the number of high-order species is larger for the labeled constructs than for the unlabeled protein, as observed in the DLS experiments (Figure S6). Nevertheless, the detection of such aggregation events at extremely low concentrations leading to subsequent fibril formation highlights the importance of these contacts in the amyloid aggregation process at physiological concentration regimens and supports a two-step nucleation mechanism.

CONCLUSIONS

SMFS techniques, particularly those utilizing multilaser methodologies, are currently capable of providing valuable insights into the mechanism of amyloid fibril formation in its elusive early stages. In this study, we have fully characterized the first step toward amyloid fibril formation for a model SH3 domain. The amyloidogenic mechanism at physiological protein concentrations, which are considerably lower than the concentrations employed in traditional studies, requires a two-step nucleation process, as recently suggested by Frenkel, Knowles, and colleagues based on coarse-grain Monte Carlo simulations.[20] These authors demonstrated the crucial role of nonspecific interactions for the first nucleation event. Our experiments lie in this range of physiologically relevant concentrations and represent direct experimental evidence of

DOI: 10.1021/acs.jpcb.5b01957
J. Phys. Chem. B XXXX, XXX, XXX−XXX

the two-step mechanism for amyloid fibrillization. In our work, we have directly detected this first step, which cannot be detected using conventional bulk techniques because of the low-concentration regimen that governs this process.

Another important point of our findings lies in the fact that this study can be expanded to other disease-related proteins. These experiments may provide the basis for designing the first line of molecular therapies to prevent aggregation by targeting the initial step of oligomerization.[38] Moreover, the effect of chaperones, other inhibitors, promoters of aggregation, and conformational changes on the monomers or the oligomers can be elegantly obtained using SMFS techniques.

■ ASSOCIATED CONTENT

Supporting Information

Detailed experimental methods; details regarding the CD, DLS, cross-linking, and additional FLIM experiments; details on the model for a loosely packed dimer; Figures S1−S7; Table S1; and complete refs 21 and 38. The Supporting Information is available free of charge on the ACS Publications website at DOI: 10.1021/acs.jpcb.5b01957.

■ AUTHOR INFORMATION

Corresponding Author

*E-mail angelort@ugr.es; Tel +34 958243825; Fax +34 958244090 (A.O.).

Notes

The authors declare no competing financial interest.

■ ACKNOWLEDGMENTS

This work is funded by grant P10-FQM-6154 from the Consejeria de Innovacion, Ciencia y Empresa (Junta de Andalucía). F.C. acknowledges the Consejeria de Innovacion, Ciencia y Empresa (Junta de Andalucía), for a PhD studentship.

■ REFERENCES

(1) Chiti, F.; Dobson, C. M. Protein Misfolding, Functional Amyloid, and Human Disease. *Annu. Rev. Biochem.* **2006**, *75*, 333−366.

(2) Knowles, T. P. J.; Vendruscolo, M.; Dobson, C. M. The Amyloid State And Its Association With Protein Misfolding Diseases. *Nat. Rev. Mol. Cell Biol.* **2014**, *15*, 384−396.

(3) Kayed, R.; Lasagna-Reeves, C. A. Molecular Mechanisms of Amyloid Oligomers Toxicity. *J. Alzheimer's Dis.* **2013**, *33*, S67−S78.

(4) Cohen, S. I. A.; Vendruscolo, M.; Dobson, C. M.; Knowles, T. P. J. From Macroscopic Measurements to Microscopic Mechanisms of Protein Aggregation. *J. Mol. Biol.* **2012**, *421*, 160−171.

(5) Knowles, T. P. J.; Waudby, C. A.; Devlin, G. L.; Cohen, S. I. A.; Aguzzi, A.; Vendruscolo, M.; Terentjev, E. M.; Welland, M. E.; Dobson, C. M. An Analytical Solution to the Kinetics of Breakable Filament Assembly. *Science* **2009**, *326*, 1533−1537.

(6) He, X.; Giurleo, J. T.; Talaga, D. S. Role of Small Oligomers on the Amyloidogenic Aggregation Free-Energy Landscape. *J. Mol. Biol.* **2010**, *395*, 134−154.

(7) Varela, L.; Morel, B.; Azuaga, A. I.; Conejero-Lara, F. A Single Mutation In An SH3 Domain Increases Amyloid Aggregation by Accelerating Nucleation, But Not by Destabilizing Thermodynamically the Native State. *FEBS Lett.* **2009**, *583*, 801−806.

(8) Paredes, J. M.; Casares, S.; Ruedas-Rama, M. J.; Fernandez, E.; Castello, F.; Varela-Alvarez, L.; Orte, A. Early Amyloidogenic Oligomerization Studied through Fluorescence Lifetime Correlation Spectroscopy. *Int. J. Mol. Sci.* **2012**, *13*, 9400−9418.

(9) Luo, J.; Wärmländer, S. K. T. S.; Gräslund, A.; Abrahams, J. P. Alzheimer Peptides Aggregate into Transient Nanoglobules That Nucleate Fibrils. *Biochemistry* **2014**, *53*, 6302−6308.

(10) Wördehoff, M. M.; Bannach, O.; Shaykhalishahi, H.; Kulawik, A.; Schiefer, S.; Willbold, D.; Hoyer, W.; Birkmann, E. Single Fibril Growth Kinetics of α-Synuclein. *J. Mol. Biol.* **2015**, *427*, 1428−1435.

(11) Esbjörner, E. K.; Chan, F.; Rees, E.; Erdelyi, M.; Luheshi, L. M.; Bertoncini, C. W.; Kaminski, C. F.; Dobson, C. M.; Kaminski-Schierle, G. S. Direct Observations of Amyloid β Self-Assembly in Live Cells Provide Insights into Differences in the Kinetics of Aβ(1−40) and Aβ(1−42) Aggregation. *Chem. Biol.* **2014**, *21*, 732−742.

(12) Joo, C.; Balci, H.; Ishitsuka, Y.; Buranachai, C.; Ha, T. Advances in Single-Molecule Fluorescence Methods for Molecular Biology. *Annu. Rev. Biochem.* **2008**, *77*, 51−76.

(13) Kapanidis, A. N.; Strick, T. Biology, One Molecule at a Time. *Trends Biochem. Sci.* **2009**, *34*, 234−243.

(14) Orte, A.; Clarke, R.; Balasubramanian, S.; Klenerman, D. Determination of the Fraction and Stoichiometry of Femtomolar Levels of Biomolecular Complexes in an Excess of Monomer Using Single-Molecule, Two-Color Coincidence Detection. *Anal. Chem.* **2006**, *78*, 7707−7715.

(15) Hillger, F.; Nettels, D.; Dorsch, S.; Schuler, B. Detection and Analysis of Protein Aggregation with Confocal Single Molecule Fluorescence Spectroscopy. *J. Fluoresc.* **2007**, *17*, 759−65.

(16) Orte, A.; Birkett, N. R.; Clarke, R. W.; Devlin, G. L.; Dobson, C. M.; Klenerman, D. Direct Characterization of Amyloidogenic Oligomers by Single-Molecule Fluorescence. *Proc. Natl. Acad. Sci. U. S. A.* **2008**, *105*, 14424−14429.

(17) Narayan, P.; Orte, A.; Clarke, R. W.; Bolognesi, B.; Hook, S.; Ganzinger, K. A.; Meehan, S.; Wilson, M. R.; Dobson, C. M.; Klenerman, D. The Extracellular Chaperone Clusterin Sequesters Oligomeric Forms of the Amyloid-β_{1-40} Peptide. *Nature Struct. Mol. Biol.* **2012**, *19*, 79−83.

(18) Chiou, A.; Hägglöf, P.; Orte, A.; Chen, A. Y.; Dunne, P. D.; Belorgey, D.; Karlsson-Li, S.; Lomas, D. A.; Klenerman, D. Probing Neuroserpin Polymerization and Interaction with Amyloid-β Peptides Using Single Molecule Fluorescence. *Biophys. J.* **2009**, *97*, 2306−2315.

(19) Fandrich, M. Oligomeric Intermediates in Amyloid Formation: Structure Determination and Mechanisms of Toxicity. *J. Mol. Biol.* **2012**, *421*, 427−440 DOI: 10.1016/j.jmb.2012.01.006.

(20) Saric, A.; Chebaro, Y. C.; Knowles, T. P. J.; Frenkel, D. Crucial Role of Nonspecific Interactions in Amyloid Nucleation. *Proc. Natl. Acad. Sci. U. S. A.* **2014**, *111*, 17869−17874.

(21) Cremades, N.; Cohen, S. I. A.; Deas, E.; Abramov, A. Y.; Chen, A. Y.; Orte, A.; Sandal, M.; Clarke, R. W.; Dunne, P.; Aprile, F. A.; et al. Direct Observation of the Interconversion of Normal and Toxic Forms of α-Synuclein. *Cell* **2012**, *149*, 1048−1059.

(22) Mannini, B.; Mulvihill, E.; Sgromo, C.; Cascella, R.; Khodarahmi, R.; Ramazzotti, M.; Dobson, C. M.; Cecchi, C.; Chiti, F. Toxicity of Protein Oligomers Is Rationalized by a Function Combining Size and Surface Hydrophobicity. *ACS Chem. Biol.* **2014**, *9*, 2309−2317.

(23) Ferreon, A. C. M.; Gambin, Y.; Lemke, E. A.; Deniz, A. A. Interplay of α-Synuclein Binding and Conformational Switching Probed by Single-Molecule Fluorescence. *Proc. Natl. Acad. Sci. U. S. A.* **2009**, *106*, 5645−5650.

(24) Trexler, A. J.; Rhoades, E. Single Molecule Characterization of α-Synuclein in Aggregation-Prone States. *Biophys. J.* **2010**, *99*, 3048−3055.

(25) Müller, B. K.; Zaychikov, E.; Bräuchle, C.; Lamb, D. C. Pulsed Interleaved Excitation. *Biophys. J.* **2005**, *89*, 3508−3522.

(26) Kudryavtsev, V.; Sikor, M.; Kalinin, S.; Mokranjac, D.; Seidel, C. A. M.; Lamb, D. C. Combining MFD and PIE for Accurate Single-Pair Förster Resonance Energy Transfer Measurements. *ChemPhysChem* **2012**, *13*, 1060−1078.

(27) Morel, B.; Varela, L.; Azuaga, A. I.; Conejero-Lara, F. Environmental Conditions Affect the Kinetics of Nucleation of Amyloid Fibrils and Determine Their Morphology. *Biophys. J.* **2010**, *99*, 3801−3810.

(28) Morel, B.; Casares, S.; Conejero-Lara, F. A Single Mutation Induces Amyloid Aggregation in the α-Spectrin SH3 Domain: Analysis

of the Early Stages of Fibril Formation. *J. Mol. Biol.* **2006**, *356*, 453−468.
(29) Wahl, M.; Erdmann, R.; Lauritsen, K.; Rahn, H. J. Hardware Solution For Continuous Time-Resolved Burst Detection Of Single Molecules In Flow. *Proc. SPIE* **1998**, *3259*, 173−178.
(30) Edel, J. B.; Eid, J. S.; Meller, A. Accurate Single Molecule FRET Efficiency Determination for Surface Immobilized DNA Using Maximum Likelihood Calculated Lifetimes. *J. Phys. Chem. B* **2007**, *111*, 2986−2990.
(31) Kapanidis, A. N.; Heilemann, M.; Margeat, E.; Kong, X.; Nir, E.; Weiss, S. Alternating-Laser Excitation of Single Molecules. In *Single Molecule Techniques. A Laboratory Manual*; Selvin, P. R., Ha, T., Eds.; Cold Spring Harbor Laboratory Press: New York, 2008.
(32) Ruzafa, D.; Morel, B.; Varela, L.; Azuaga, A. I.; Conejero-Lara, F. Characterization of Oligomers of Heterogeneous Size as Precursors of Amyloid Fibril Nucleation of an SH3 Domain: An Experimental Kinetics Study. *PLoS One* **2012**, *7*, e49690.
(33) Ruedas-Rama, M. J.; Alvarez-Pez, J. M.; Orte, A. Solving Single Biomolecules by Advanced FRET-Based Single-Molecule Fluorescence Techniques. *Biophys. Rev. Lett.* **2013**, *08*, 161−190.
(34) Vega, M. C.; Martinez, J. C.; Serrano, L. Thermodynamic and Structural Characterization of Asn and Ala Residues in the Disallowed II′ Region of the Ramachandran Plot. *Protein Sci.* **2000**, *9*, 2322−2328.
(35) ATTO-Tec Förster-Radius of ATTO-Dye-Pairs for FRET. https://www.atto-tec.com/index.php?id=65&L=1 (accessed May 2015).
(36) Wilkins, D. K.; Grimshaw, S. B.; Receveur, V.; Dobson, C. M.; Jones, J. A.; Smith, L. J. Hydrodynamic Radii of Native and Denatured Proteins Measured by Pulse Field Gradient NMR Techniques. *Biochemistry* **1999**, *38*, 16424−16431.
(37) Casares, S.; Sadqi, M.; Lopez-Mayorga, O.; Martinez, J. C.; Conejero-Lara, F. Structural Cooperativity in the SH3 Domain Studied by Site-Directed Mutagenesis And Amide Hydrogen Exchange. *FEBS Lett.* **2003**, *539*, 125−30.
(38) Cohen, S. I. A.; Arosio, P.; Presto, J.; Kurudenkandy, F. R.; Biverstål, H.; Dolfe, L.; Dunning, C.; Yang, X.; Frohm, B.; Vendruscolo, M.; et al. A Molecular Chaperone Breaks the Catalytic Cycle that Generates Toxic Aβ Oligomers. *Nat. Struct. Mol. Biol.* **2015**, *22*, 207−213.

DOI: 10.1021/acs.jpcb.5b01957
J. Phys. Chem. B XXXX, XXX, XXX−XXX